Nonlinear Stability Analysis of a Reduced-Order Wind Turbine VSC-grid model Operating in Weak Grid Conditions

Sujay Ghosh, Guangya Yang
Technical University of Denmark
Anker Engelunds Vej 1, 2800, Denmark
Email: sujgh@elektro.dtu.dk

Mohammad Kazem B. Dowlatabadi,
Lukasz Kocewiak
Ørsted
Nesa Allé 1, 2820, Denmark

***Abstract*—In a wind turbine generator (WTG), the behaviour of the Phase-Locked Loop (PLL) under weak grid conditions becomes complex and requires nonlinear analysis to assess the WTG control performance and system stability. This paper introduces a quasi-static reduced-order VSC-grid model of a WTG and evaluates its performance for large-signal disturbances such as changes in current set points and grid short circuit ratio. The time-domain expression for a synchronous reference frame PLL is considered with its nonlinearity intact. Based on the analytical model, a V-δ mechanism is established to identify the PLL synchronisation instability events relevant to a WTG operation. Further, for PLL stable operation, a globally valid stability boundary is discussed. The complex nonlinear PLL dynamics are addressed using phase portraits, where it is shown that the results have direct implications on robust PLL gain tuning guidelines.**

I. Introduction

As a result of the rapid technological development of renewable power generations such as wind turbines and solar panels, more grid-interfaced power electronic converters are being deployed to serve the power demand. However, unlike fossil fuel power plants based on synchronous machines, the power converter interfaced generations exhibit complex transient behaviour under grid disturbances [1][2]. Hence, to ensure the uninterrupted operation and stability of the modern power systems, renewable power plants must maintain synchronism with the grid even under inevitable grid disturbances.

In a WTG, the information about the instantaneous grid voltage, phase angle and frequency is obtained from the Phase Locked Loop (PLL), which is of vital importance to maintain synchronism and stable operation of the WTG [3]. However, the behaviour of the PLL under weak grid conditions becomes complex which can not be represented by simplified linear PLL models. This presents the importance of considering the PLL nonlinear characteristics and the subsequent need for analytical methods for its analysis under weak grid conditions.

The PLL is modeled together with the WTG grid side converter. The linearised model-based approach, such as eigenvalue analysis [4]-[6] or impedance-based stability analysis [7]-[9], assumes the entire system (including WTG grid side converter and the connected power system) has a linear behavior under small disturbances, and synchronization is enforced within the vicinity of the operating point. As a result, the stability of the system cannot be valid under large disturbances or increased nonlinearity of the system.

Conversely, the nonlinear approach to stability includes large-signal disturbance and can provide global asymptotic stability conclusions [10]-[14]. The traditional Lyapunov method [10] can be used to evaluate the nonlinear stability of a WTG system, wherein an energy function can be developed, such that a decrease in energy results in the state trajectories to converge at an equilibrium point. However, due to the absence of a generalised methodology, it is difficult to develop an energy function for an arbitrary system of equations. In [11], the transient stability based on the equal-area criterion is evaluated and presents that during transients, the PLL is destabilized by large disturbances in the grid.

In [12], the PLL differential equation is represented as a dissipative Hamiltonian system that provides a better understanding of the nonlinear dynamics. An analytical approach based on describing function and generalized Nyquist criterion is proposed in [13], where the nonlinear components are represented by approximated describing function to estimate the sub-synchronous oscillations. The concept of the Passivity index is used in [14], which quantifies the excess or shortage of passivity of a nonlinear WTG system, which is closely associated with stability.

The nonlinear stability methods described in [10]-[14] need detailed converter and network models including nonlinear components such as saturation, dead-band, etc. which adds to the computation burden. The existing literature is also lacking in systematic PLL transient synchronization stability assessment methods, considering the nonlinear effects of the system. The main contribution in this paper includes (1) introduction to a quasi-static reduced-order model of the WTG system and evaluation of its performance for large-signal disturbances under weak grid conditions, (2) establish the V-δ mechanism to identify the PLL instability events relevant to a WTG operation, and (3) quantify the PLL stable operating boundary valid globally.

II. Wind turbine model

The system under study is a grid side converter of type-4 WTG, whose schematic diagram is shown in Fig. 1. It is considered that the current is controlled on the converter side inductance, while the filter bus voltage is measured for

synchronizing the VSC with the grid through the PLL. The control diagram of the synchronous reference frame PLL used is presented in Fig. 2, and the set of system and control parameters as per [15] are listed in Table I.

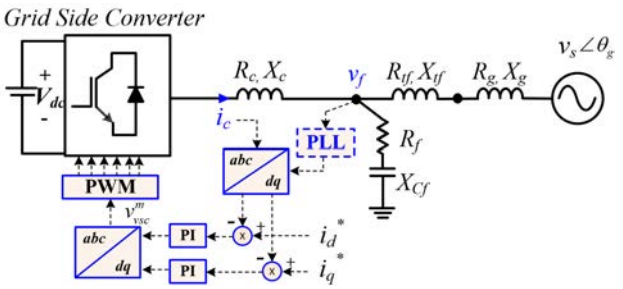

Fig. 1. Single-line diagram of a grid-connected VSC using the typical vector current control.

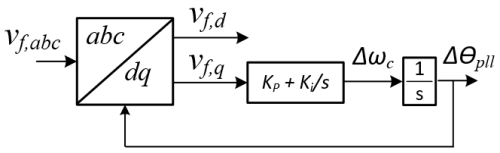

Fig. 2. Block diagram of the SRF-PLL.

TABLE I
SYSTEM AND CONTROL PARAMETERS IN FIG. 1.

Symbol	Description	Value
S_b	Rated power	12 MVA
V_s	Nominal grid voltage (L-N, pk)	$690\sqrt{2/3}$ V
V_{dc}	DC-link voltage	1.38 kV
f_0	Rated frequency	50 Hz
f_{sw}	Switching frequency	2950 Hz
f_s	Sampling frequency	$2 \cdot f_{sw}$
R_c, X_c	Converter-side inductor (pu)	0.005, 0.105
R_{tf}, X_{tf}	Grid-side inductor (pu)	0.005, 0.1
R_f, X_{cf}	Filter capacitor (pu)	0.03, 0.075
R_g, X_g	Grid impedance	SCR=3&1.2, X/R=20
K_{cc}	Current controller Kp Ki	0.2, 5
K_{pll}	Initial PLL design of Kp Ki	0.1, 10

A. Quasi-static reduced order model

Based on the principle of reduced-order modelling, the fast dynamics of a system can be neglected when studying the impact of slow dynamics [16]. Since the bandwidth of the inner current loop is much higher than that of the PLL, the grid side converter can be simplified as a controlled current source which precisely follows the current reference as shown in Fig. 3.

As per Fig. 2, the dynamic equation of the PLL is,

$$\Delta\theta_{PLL} = \int (Kp + Ki\int) \cdot v_{f_q} \tag{1}$$

where, Kp and Ki are the proportional and integral gain of the PI regulator, respectively. While v_{f_q} represents the q-axis component of the filter bus voltage in PLL coordinates. From Fig. 3, v_{f_q} could be simply expressed by superposition principle, as the voltage contributed from the voltage source and the current source, simultaneously. The v_f due to voltage

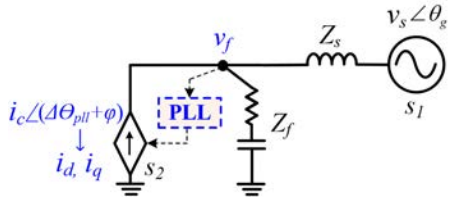

Fig. 3. Reduced order VSC-grid system for stability analysis.

source (s1) can be written as,

$$v_{f_{s1}} = \frac{Z_f(\omega_n)}{Z_f(\omega_n) + Z_s(\omega_n)} \cdot V_s\angle\theta_g \Rightarrow k_v(\omega_n) \cdot V_s\angle\Delta\theta_g^{'} \tag{2}$$

where, $k_v(\omega_n) = abs(Z_f(\omega_n)/[Z_f(\omega_n) + Z_s(\omega_n)])$, $\Delta\theta_g^{'} = (\theta_g + \angle Z_f(\omega_n)/[Z_f(\omega_n) + Z_s(\omega_n)])$ and ω_n is the nominal grid frequency. Considering dq transform where phase A vector is initially aligned to d-axis, the q-component of $v_{f_{s1}}$ derived in (2) can be written as,

$$v_{f_{s1,q}} = k_v(\omega_n) \cdot V_s \cdot \sin(\Delta\theta_g^{'} - \Delta\theta_{PLL}) \tag{3}$$

Similarly, from Fig. 3, the v_f due to the current source (s2) can be simply expressed as the voltage drop across Z_s. In general, from static analysis of the dynamic current equation of an impedance $Z(= R + j \cdot X)$, the q-axis voltage can be obtained as,

$$v_{zq} = R \cdot i_q^{'} + X \cdot i_d^{'} \tag{4}$$

where, $i_d^{'}$ and $i_q^{'}$ are dq-axis current through Z. Therefore, if i_d and i_q are the converter reference currents, based on (4) and current divider formula, the q-component of $v_{f_{s2}}$ can be written as,

$$v_{f_{s2,q}} = k_c(\omega_c) \cdot [R_s \cdot i_q + X_s(\omega_c) \cdot i_d] \tag{5}$$

where, $k_c(\omega_c) = Z_f(\omega_c)/[Z_f(\omega_c) + Z_s(\omega_c)]$, and ω_c is the PLL frequency. Subsequently, the filter bus voltage v_{f_q} can be written as,

$$v_{f_q} = v_{f_{s1,q}} + v_{f_{s2,q}} \tag{6}$$

Substituting (3), (5) and (6) into (1), and defining $\delta = (\Delta\theta_{PLL} - \Delta\theta_g^{'})$ yields,

$$\Delta\theta_{PLL} = \int (Kp + Ki\int) \cdot (-k_v(\omega_n) \cdot V_s \sin\delta + k_c(\omega_c) \cdot [i_q R_s + i_d X_s(\omega_c)]) \tag{7}$$

Thus, the second-order PLL considering the reduced VSC–grid model can be characterized by (7) and can be drawn as per Fig. 4.

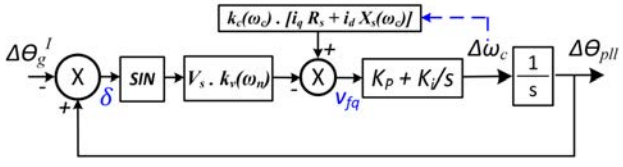

Fig. 4. Equivalent diagram of the reduced VSC–grid model.

B. System Equilibrium points

1) Existence of Equilibrium points: The PLL synchronisation stability of the reduced order VSC–grid model described in (7) requires the existence of equilibrium points, i.e. at steady-state (6) must be zero (v_{f_q} = 0), leading to

$$k_v(\omega_n) \cdot V_s \sin\delta = k_c(\omega_c) \cdot [i_q R_s + i_d X_s(\omega_c)] \quad (8)$$

The analytical expression in (8) could be graphically analysed as per Fig. 5a, where it is evident that the existence of the solution of (8) requires

$$\mid k_v(\omega_n) \cdot V_s \mid \geq \mid k_c(\omega_c) \cdot [i_q R_s + i_d X_s(\omega_c)] \mid \quad (9)$$

For an operating condition, there exist two equilibrium points, 'a' and 'b'. The equilibrium points are affected by the active current and reactive current, the grid impedance, and the grid voltage magnitude (only electrical quantities not controller gains). The PLL synchronisation instability will be inevitable if there is no equilibrium point, also it may occur if system is attracted to point 'b' in Fig. 5a.

2) Local Stability of Equilibrium Point: Before analysing the transient stability of the reduced order VSC–grid model, one must assure that the system is small-signal stable at the equilibrium points 'a' and 'b', as in Fig. 5a. This is done by checking the eigenvalues of the linearized state matrix of the system.

The linear approximation of the model described in (7), where the higher-order terms are neglected, reduces to

$$\begin{bmatrix} \dot{r_{pi}} \\ \Delta\dot{\theta}_{pll} \end{bmatrix} = \begin{bmatrix} 0 & -\mid k_v \mid Ki_{pll} V_s cos(\angle k_v - \theta_{pll0}) \\ 1 & -\mid k_v \mid Kp_{pll} V_s cos(\angle k_v - \theta_{pll0}) \end{bmatrix} \begin{bmatrix} r_{pi} \\ \Delta\theta_{pll} \end{bmatrix} + \begin{bmatrix} Ki_{pll} X_s k_c & Ki_{pll} R_s k_c \\ Kp_{pll} X_s k_c & Kp_{pll} R_s k_c \end{bmatrix} \begin{bmatrix} i_d \\ i_q \end{bmatrix} \quad (10)$$

r_{pi} is the state variable of the PI regulator, θ_{pll0} is the steady state PLL angle, while other parameters are as per section II-A. Considering a current reference of $i_d = 13kA$ and $i_q = -1.5kA$, the eigenvalues for state matrix in (10) with varying grid impedance is illustrated in Fig. 5b. Qualitative change within system refers to the shift that occurs when a system goes from one attractor state through an instability into a different attractor state.

From Fig. 5, it is seen that for point 'a' the eigenvalues are complex with negative real part. On the other hand, for point 'b' the eigenvalues are real with one positive and one negative value. As per linear system theory, stability can only be guaranteed for equilibrium points having eigenvalues with strictly negative real part. Hence, if the system is attracted to the point 'b', the system is unstable, whereas at point 'a' the system is always stable. However, linear analysis cannot quantify the domain of attraction, i.e. if the initial condition is very far from point 'a', the stability is still not guaranteed.

C. Short circuit ratio vs Damping ratio

From Fig. 4, the linearized closed-loop transfer function of the reduced VSC-grid model can be written as,

$$\frac{\Delta\delta}{\Delta v_{f_q}} = \frac{M_1}{s^2 + M_2 s + M_3} \quad (11)$$

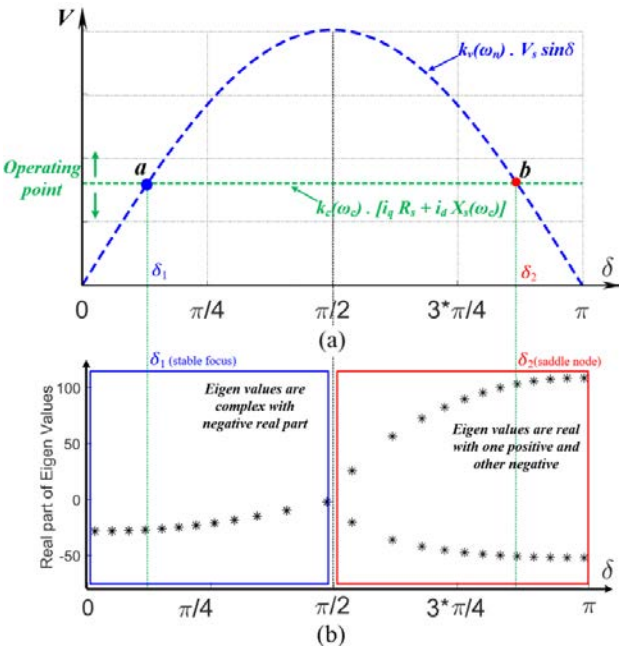

Fig. 5. (a) Existence of equilibrium points, (b) Eigenvalue analysis with varing grid impedance. Equilibrium point 'a' is a stable focus, i.e stable point. Whereas, the equilibrium point 'b' is a saddle node, i.e unstable point.

M1, M2 and M3 are shown in (12)

$$\begin{aligned} M_1 &= (Kp_{pll} s + Ki_{pll}) \cdot (V_s k_{v,\delta_0} - k_{c,\delta_0}[i_q R_s + i_d X_s]) \\ M_2 &= Kp_{pll} \cdot (V_s k_{v,\delta_0} - k_{c,\delta_0}[i_q R_s + i_d X_s]) \\ M_3 &= Ki_{pll} \cdot (V_s k_{v,\delta_0} - k_{c,\delta_0}[i_q R_s + i_d X_s]) \end{aligned} \quad (12)$$

where, $k_{v,\delta_0} = k_v(\omega_{\delta_0})$, $k_{c,\delta_0} = k_c(\omega_{\delta_0})$ and δ_0 is the PLL angle equilibrium point. From (11), the damping ratio of the second order system that varies with operating conditions is given by,

$$\begin{aligned} \zeta &= \frac{M_2}{2\sqrt{M_3}} \\ &= \frac{Kp_{pll}\sqrt{(V_s k_{v,\delta_0} - k_{c,\delta_0}[i_q R_s + i_d X_s])}}{2\sqrt{Ki_{pll}}} \end{aligned} \quad (13)$$

Under the assumption of a stable grid voltage, the short-circuit ratio (SCR) defines the magnitude of the line current and the grid impedance values [17], and can be expressed as

$$SCR = \frac{3V_s^2}{Z_s \cdot S_b} = \frac{V_s}{I_L \cdot Z_s} \Rightarrow \frac{V_s k_{v,\delta_0}}{k_{c,\delta_0}[i_q R_s + i_d X_s(\omega_c)]} \quad (14)$$

where S_b is the output power of the grid-connected converter. Substituting (14) into (13), the damping ratio can be expressed as (15), where the variation of damping with SCR is shown in Fig. 6.

$$\zeta = \frac{Kp_{pll}\sqrt{(1 - \frac{1}{SCR})}}{2\sqrt{\frac{Ki_{pll}}{V_s k_{v,\delta_0}}}} \quad (15)$$

Fig. 6, shows that when the SCR drops below 1.5, the system damping drops sharply. This is extremely detrimental to the stability of the reduced VSC-grid model.

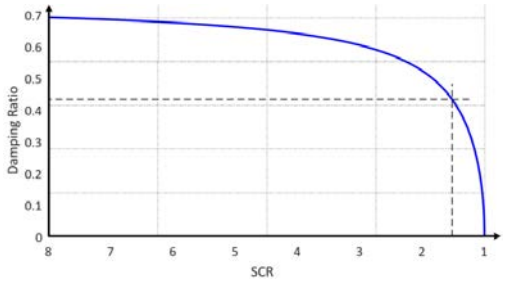

Fig. 6. Damping ratio of reduced VSC-grid model versus SCR, $Kp_{pll} = 0.1$ and $Ki_{pll} = 10$. Optimal damping at SCR = 8.

III. TRANSIENT STABILITY ANALYSIS

Even though a system is locally stable at the equilibrium points, it is far from certain that the system will converge to this stable point considering a large disturbance. In this paper, large disturbances in the filter bus voltage are caused by changes in the grid-side impedance or changes in the WTG reference current.

A. Model validation

Before carrying out the transient stability analysis, the time response of the reduced VSC-grid model must be validated against the detailed WTG model as described in Fig. 1 and Table 1. The q-axis voltage at the filter bus and the angle tracked by the PLL are presented in Fig. 7.

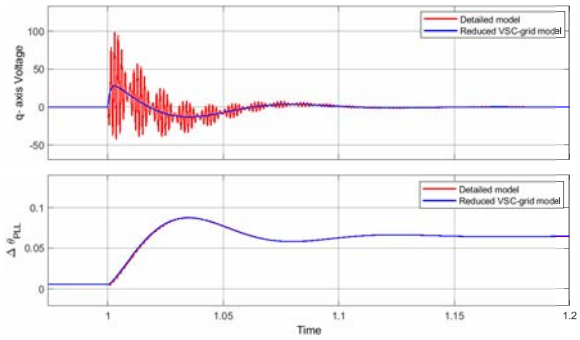

Fig. 7. Detailed simulation model vs Reduced order analytical model: q-axis filter bus voltage and the angle tracked by the PLL.

Post disturbance, it can be observed that the time response of the reduced VSC-grid model is somewhat similar to that of the detailed VSC model. During transients, a high-frequency oscillation is seen in the filter bus voltage for the detailed VSC model, which is determined as the LC natural frequency. This high frequency is not reflected in the reduced model, hence, it can be deduced that the derived model is valid for low-frequency instability events. The angle tracked by the PLL is exactly the same for both the models.

B. Identification of Unstable PLL synchronisation events, and its boundary

There are two scenarios of PLL transient synchronization instability. Fig. 8a represents the scenario when the operating point is high (lower margin between b and b'). Whereas, Fig. 8b represents the scenario when the operating point is low (higher margin between c and c'). For both scenarios, the system initially operates at 'a', and then a large disturbance leads the system to either b/c (stable) or beyond b'/c' (unstable). The sequence of the events described is as follows,

1) Post disturbance, if the output frequency of the PLL recovers to the grid frequency before reaching b'/c', then the PLL retraces the $k_v(\omega_n)V_s sin\delta$ curve and reaches b/c after several cycles of oscillation, resulting in a stable system.
2) Conversely, if the output frequency of the PLL is below the grid frequency as it reaches b'/c'. Then, the output frequency keeps decreasing beyond b'/c', and the system eventually loses synchronism with the grid.

The loss of synchronism could be either represented as the red curve, which is similar to the conventional 'first swing angle instability', or the blue curve which corresponds to the 'multi-swing angle instability' discussed in [17]. A detailed analysis is carried out in the following section.

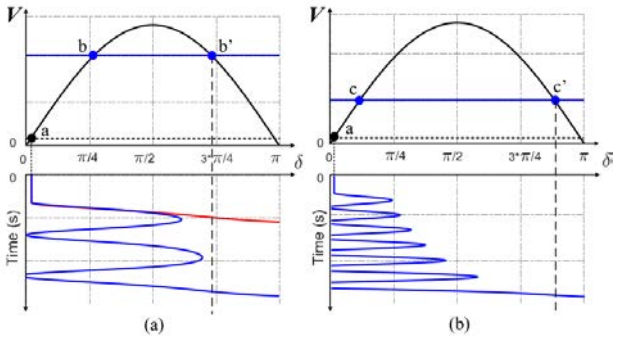

Fig. 8. Unstable PLL synchronisation scenario: (a) higher operating point, (b) lower operating point. Instability classified as 1st or multi swing instability.

C. Phase plane analysis

Instead of individually analysing several time-domain simulations, one can use phase portraits to analyze a large amount of different initial conditions and graphically visualize the trajectory of each solution in the phase-plane. In this paper, the initial conditions are perturbed by sweeping the PLL gains. From this, one can determine the required PLL tuning for the system to survive a large-signal disturbance.

1) Scenario 1: In Fig. 9 and 10, the trajectories of the system under high grid impedance and large converter current jump is visualized for different values of PLL controller gain. A short circuit ratio of 1.2 (X/R=20) is considered with a current jump (rise time $\approx$ 5ms) of 1kA to 13kA.

In the figures, the color code indicates varying PLL gains as one goes from blue towards red. Four stages of operation can be observed in scenario-1. For low values of Kp or higher values of Ki, the system is found to be unstable. This is also validated from (15), where it can be established that low values of Kp or higher values of Ki, results in lower damping. Fig. 9b and 9c, represents the first swing angle instability and multi-swing angle instability, respectively. It must be noted that from small-signal analysis, for the PLL controller gains stated in Fig. 9b and 9c, the instability is not observed. Yet, as shown in Fig. 9b and 9c, the system is transiently unstable. Hence, a nonlinear analysis must be used to detect this event.

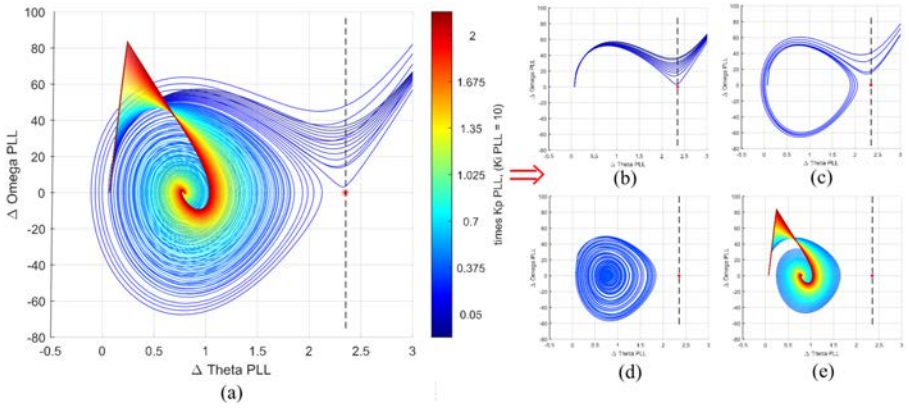

Fig. 9. Phase portrait for scenario-1: increasing Kp_{pll} (blue to red). (a) 0.05 to 2 times Kp_{pll}, (b) Stage-1: 0.05 to 0.26 times Kp_{pll}, (c) Stage-2: 0.28 to 0.36 times Kp_{pll}, (d) Stage-3: 0.38 to 0.50 times Kp_{pll}, and (e) Stage-4: 0.52 to 2 times Kp_{pll}.

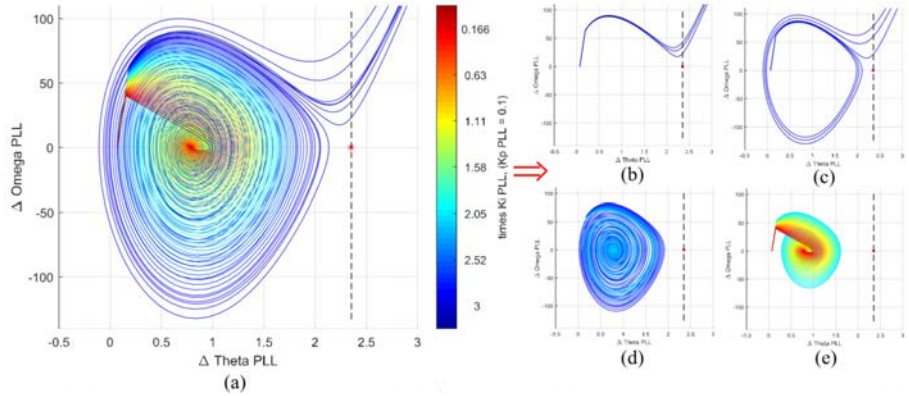

Fig. 10. Phase portrait for scenario-1: decreasing Ki_{pll} (blue to red). (a) 3 to 0.16 times Ki_{pll}, (b) Stage-1: 3 to 2.88 times Ki_{pll}, (c) Stage-2: 2.83 to 2.69 times Ki_{pll}, (d) Stage-3: 2.64 to 2 times Ki_{pll}, and (e) Stage-4: 1.9 to 0.16 times Ki_{pll}.

The cause of first swing angle instability is mainly due to higher operating point, such that a large disturbance directly pushes the system beyond the stability boundary b'/c'. Whereas, the cause of multi swing angle instability is mainly due to improper tuning of the PLL controller gains.

Further, Fig. 9d represents the condition when the system is oscillatory, i.e. several cycles of oscillation is observed before the system stabilises to an equilibrium. The frequency of the oscillation observed is approx. 9 Hz. Finally, Fig. 9e resembles a stable focus, where with higher values of Kp, lower settling time is observed, i.e. the system reaches equilibrium quickly. A similar set of phase portraits is seen in Fig. 10 a-e.

2) Scenario 2: In scenario-2, a short circuit ratio of 3 (X/R=20) is considered with a current jump (rise time $\approx$ 5ms) of 1kA to 13kA. Similarly, the trajectories of the system are visualized for different values of PLL controller gain. From Fig. 11 and 12, it is seen that compared to scenario-1, only three stages of operation is observed. Since the operating point is lower, first swing angle instability is not observed. The observations in the rest of the stages are similar to the discussion presented in scenario-1.

D. Time-domain verification of Phase plane plots

To conclude that the phase-plane analysis of the reduced VSC-grid model provides a valid stability conclusion for the detailed WTG grid converter model described in Fig. 1 and Table 1, the time-domain simulation of two instabilities, namely first swing angle instability in scenario-1 and multi-swing angle instabilty in scenario-2 is shown in Fig 13 and Fig. 14, respectively. The Kp_{pll} and Ki_{pll} values are taken from the respective phase portraits and used in the detailed WTG model to validate the results. The simulation results are divided into three subfigures with q-axis filter bus voltage, $\Delta\theta_{pll}$ and converter reference currents i_d and i_q representing the large signal disturbance.

In Fig. 13, it can be clearly seen that the large current jump results in the $\Delta\theta_{pll}$ to cross the stability boundary ($\Delta\theta_{pll} = 2.35rad$) in first swing. Subsequently, the time at which the $\Delta\theta_{pll}$ escapes, the q-axis filter bus voltage destabilises.

Similarly, in Fig. 14, it can be seen that the large current jump results in the $\Delta\theta_{pll}$ to heavily oscillate (multi swing), and thereafter crosses the stability boundary ($\Delta\theta_{pll} = 2.35rad$). Subsequently, the time at which the $\Delta\theta_{pll}$ escapes, the q-axis filter bus voltage destabilises.

E. Recommendation for PLL synchronisation reliability

From the previous analysis, it is shown that for a large disturbance, the system transient stability depends on several factors such as X/R ratio of the grid, voltage at the grid bus, impedance of the WTG transformer and LCL filter, and operating point of the WTG. Despite several factors, a system designer often has some information such as bounds on the short-circuit ratio and the typical design of the WTG.

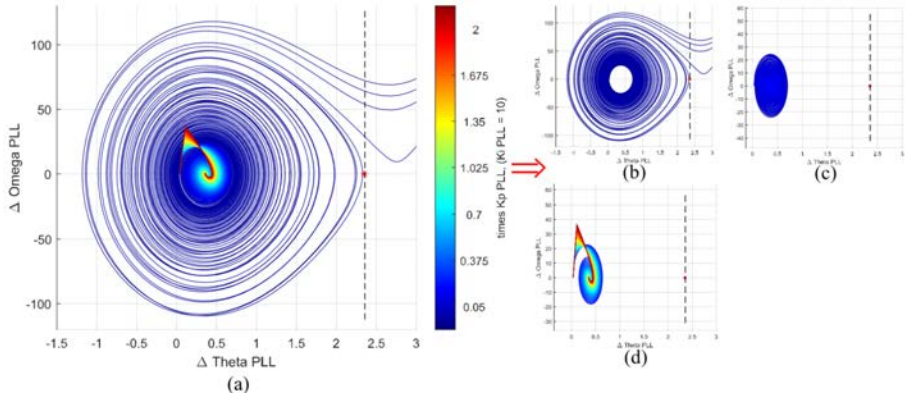

Fig. 11. Phase portrait for scenario-2: increasing Kp_{pll} (blue to red). (a) 0.05 to 2 times Kp_{pll}, (b) Stage-1: 0.05 to 0.11 times Kp_{pll}, (c) Stage-2: 0.13 to 0.30 times Kp_{pll}, and (d) Stage-3: 0.32 to 2 times Kp_{pll}.

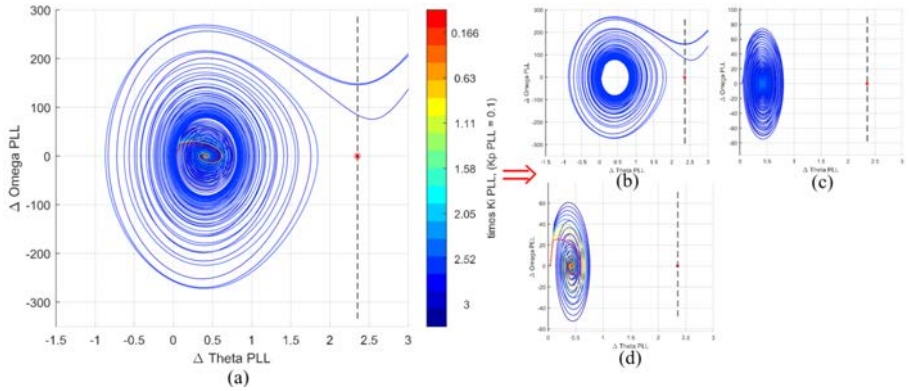

Fig. 12. Phase portrait for scenario-2: decreasing Ki_{pll} (blue to red). (a) 3 to 0.16 times Ki_{pll}, (b) Stage-1: 3 to 2.82 times Ki_{pll}, (c) Stage-2: 2.69 to 2.50 times Ki_{pll}, and (d) Stage-3: 2.44 to 0.16 times Ki_{pll}.

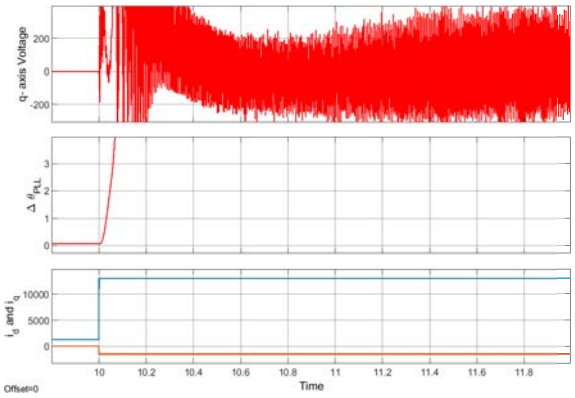

Fig. 13. Results from detailed simulation model. First swing angle instability in scenario-1 (SCR=3) with 0.05 times Kp_{pll}.

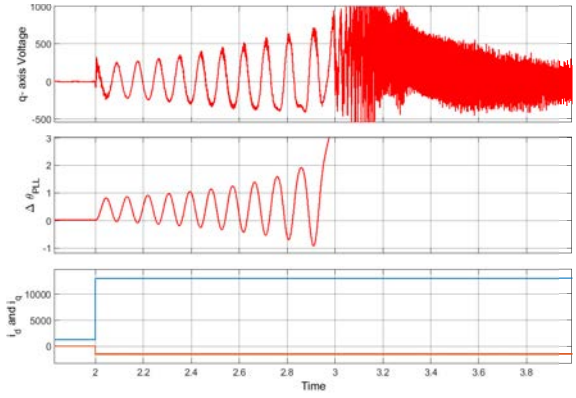

Fig. 14. Results from detailed simulation model. Multi swing angle instability in scenario-2 (SCR=1.2) with 0.2 times Kp_{pll}.

From the study it shows that it is possible with the reduced VSC-grid model to select a set of PLL controller parameters to ensure PLL synchronisation reliability.

Further, it was proven that higher values of Kp_{pll} and lower values of Ki_{pll} can enhance system stability if equilibrium points exists. Where, the lower bound on Kp_{pll} or upper bound on Ki_{pll} can be decided based on distance from stability boundary as shown in the phase portrait analysis. However, it is also important to put an upper limit on Kp_{pll} and lower limt on Ki_{pll}.

Fig. 15 presents the bode plot of the reduced VSC-grid model obtained from (11). Blindly increasing the Kp_{pll} to stabilise the system naturally increases the PLL bandwidth. Higher PLL bandwidth is undesirable because of the limited bandwidth of the inner current controller. Under such circumstance, instability may occur when the time constants between the two loops are comparable. On the other hand, decreasing Ki_{pll} is a prominent way of increasing the system stability. However one must be also careful, so that the time constants of the outer voltage loop and PLL does not become comparable.

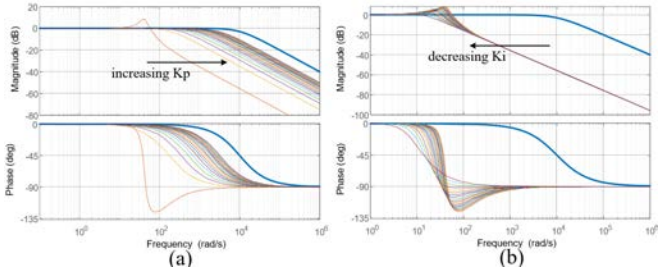

Fig. 15. Bode plots: (a) increasing Kp_{pll}, (b) decreasing Ki_{pll}. Bold blue line represents a illustrative current controller bode plot.

IV. Conclusion

This paper presented a quasi-static reduced-order model of the WTG grid converter system and evaluated its performance for large-signal disturbances under weak grid conditions. The following was concluded:

1) The nonlinear quasi-static reduced-order VSC-grid model derived in the paper closely resembles the actual WTG model in the low frequency range, which is sufficient for PLL transient synchronisation stability conclusions.
2) The PLL synchronisation instability is inevitable if there is no equilibrium point or presence of unstable equilibrium points. The unstable equilibrium points could be evaluated from small-signal stability analysis. However, it is shown that even though the system may be locally stable at the equilibrium points, it is far from certain that the system will be attracted to these point considering a large-signal disturbance.
3) The second-order characteristics of the derived reduced model allows phase portrait analysis, which enables to visualize the nonlinear stability for a large amount of different initial conditions. From the results, it is seen that such analysis is adequate to conclude the synchronisation stability of the detailed WTG model.
4) Two kinds of PLL instability events exist. The cause of 'first swing angle instability' is mainly due to higher operating point, such that a large disturbance directly pushes the system beyond the stability boundary. Whereas, the cause of 'multi swing angle instability' is mainly due to improper tuning of the PLL controller gains.
5) Higher values of Kp_{pll} and lower values of Ki_{pll} can enhance PLL synchronisation stability if equilibrium points exists. However, instability may occur when the time constants between the PLL and the inner current loop or the outer voltage loop are comparable.

The systematic approach to stability assessment brings a better understanding of the PLL stability under weak grid conditions. However, the following future work is needed:

1) The VSC-grid model could be adapted with realistic offshore grid network parameters including the outer loop control for the WTG grid converter.
2) The nonlinear components such as frequency limiters could be included in the future version of the model and its impact on PLL transient instability could be studied.
3) The PLL synchronisation instability could be extended for fault analysis for the WTG. Wherein, the dynamics of the fault current contributed from the WTG and the grid codes must be considered.

References

[1] D. Wang, J. L. Rueda Torres, A. Perilla, E. Rakhshani, P. Palensky and M. A. A. M. van der Meijden, "Enhancement of Transient Stability in Power Systems with High Penetration Level of Wind Power Plants," 2019 IEEE Milan PowerTech, 2019, pp. 1-6.

[2] Y. Li et al., "PLL Synchronization Stability Analysis of MMC-Connected Wind Farms Under High-Impedance AC Faults," in IEEE Transactions on Power Systems, vol. 36, no. 3, pp. 2251-2261.

[3] L. N. Arruda, S. M. Silva and B. J. C. Filho, "PLL structures for utility connected systems," Conference Record of the 2001 IEEE Industry Applications Conference. 36th IAS Annual Meeting (Cat. No.01CH37248), 2001, pp. 2655-2660 vol.4.

[4] J. Ma, Y. Qiu, Y. Li, W. Zhang, Z. Song and J. S. Thorp, "Research on the Impact of DFIG Virtual Inertia Control on Power System Small-Signal Stability Considering the Phase-Locked Loop," in IEEE Transactions on Power Systems, vol. 32, no. 3, pp. 2094-2105, May 2017.

[5] J. Hu, Q. Hu, B. Wang, H. Tang and Y. Chi, "Small Signal Instability of PLL-Synchronized Type-4 Wind Turbines Connected to High-Impedance AC Grid During LVRT," in IEEE Transactions on Energy Conversion, vol. 31, no. 4, pp. 1676-1687, Dec. 2016.

[6] Wu, F., Zhang, X.-P., Godfrey, K., Ju, P. "Small signal stability analysis and optimal control of a wind turbine with doubly fed induction generator", (2007) IET Generation, Transmission and Distribution, 1 (5), pp. 751-760.

[7] Liu, H., Sun, J. "Voltage stability and control of offshore wind farms with AC collection and HVDC transmission", (2014) IEEE Journal of Emerging and Selected Topics in Power Electronics, 2 (4), art. no. 6914527, pp. 1181-1189.

[8] Huang, P.-H., El Moursi, M.S., Xiao, W., Kirtley, J.L. "Subsynchronous resonance mitigation for series-compensated dfig-based wind farm by using two-degree-of-freedom control strategy", (2015) IEEE Transactions on Power Systems, 30 (3), art. no. 6887372, pp. 1442-1454.

[9] Amin, M., Molinas, M. "Understanding the Origin of Oscillatory Phenomena Observed between Wind Farms and HVdc Systems", (2017) IEEE Journal of Emerging and Selected Topics in Power Electronics, 5 (1), art. no. 7605516, pp. 378-392.

[10] Vu, T.L., Turitsyn, K. "Lyapunov Functions Family Approach to Transient Stability Assessment", (2016) IEEE Transactions on Power Systems, 31 (2), art. no. 7106572, pp. 1269-1277.

[11] G. Han, C. Zhang, and X. Cai, "Mechanism of frequency instability of full-scale wind turbines caused by grid short circuit fault and its control method," Trans. China Electrotech. Soc., vol. 33, no. 10, pp. 2168–2174, May 2018.

[12] M. Bravo, A. Garcés, O. D.Montoya, and C. R. Baier, "Nonlinear analysis for the three-phase PLL: A new look for a classical problem," in Proc. IEEE Workshop Control Model. Power Electron., Padua, Italy, Jun. 2018, pp. 1–6.

[13] Y. Xu, Z. Gu and K. Sun, "Characterization of Subsynchronous Oscillation with Wind Farms Using Describing Function and Generalized Nyquist Criterion," in IEEE Transactions on Power Systems, vol. 35, no. 4, pp. 2783-2793, July 2020.

[14] P. Yang, F. Liu, Z. Wang, C. Shen, J. Yi, and W. Lin, "Toward distributed stability analytics for power systems with heterogeneous bus dynamics," arXiv preprint arXiv:1908.00752, 2019.

[15] Ł. Kocewiak, R. Blasco-Giménez, C. Buchhagen, J. B. Kwon, Y. Sun, A. Schwanka Trevisan, M. Larsson, X. Wang, "Overview, Status and Outline of Stability Analysis in Converter-based Power Systems," in Proc. The 19th International Workshop on Large-Scale Integration of Wind Power into Power Systems as well as Transmission Networks for Offshore Wind Farms, Energynautics GmbH, 11-12 November 2020.

[16] Y. Gu, N. Bottrell, and T. C. Green, "Reduced-order models for representing converters in power system studies," IEEE Trans. Power Electron., vol. 33, no. 4, pp. 3644–3654, Apr. 2018.

[17] J. Zhao, M. Huang, H. Yan, C. K. Tse and X. Zha, "Nonlinear and Transient Stability Analysis of Phase-Locked Loops in Grid-Connected Converters," in IEEE Transactions on Power Electronics, vol. 36, no. 1, pp. 1018-1029, Jan. 2021.